Ion-induced electron emission from surfaces: Dynamical screening effects

Konstantin A. Kouzakov* and Jamal Berakdar
Max-Planck-Institute of Microstructure Physics, Weinberg 2, 06120 Halle, Germany
(Received 12 April 2003; published 22 August 2003)

A theoretical model is developed for the description of the single-electron emission from surfaces following the impact of fast ions. The theory describes quantum mechanically the ion reflection at the surface and the excitation of the valence band electrons via an ion-electron interaction renormalized by the dielectric response of the target. Numerical calculations are presented and analyzed for the electron emission from the conduction band of an aluminum surface upon proton impact. Particular attention is devoted to the influence of the dielectric screening on the energy distributions and the angular distributions of the ejected electrons. In addition, the role of the surface electronic structure is studied.

DOI: 10.1103/PhysRevA.68.022902 PACS number(s): 34.50.Dy, 79.20.Rf, 34.50.Bw

I. INTRODUCTION

The electron emission is a fundamental phenomenon that can be induced by the scattering of ions from a solid target [1–3]. The electron ejection from a condensed sample can be viewed as a three-step process [4]: (1) the generation of excited electrons, (2) the electron transport through the solid including cascade multiplications, and (3) the escape of some of the electrons into the vacuum. Measurements of the energy and the angular distributions of the electrons in coincidence with the scattered projectile allow a disentanglement of the direct single-electron emission processes from those accompanied by the generation of cascade secondary electrons. This is achieved by means of the energy and wave-vector conservation laws. In recent years, remarkable advances have been made in the development and utilization of coincidence techniques for the study of the ion-induced electron emission from surfaces [5–7], even though, to our knowledge, a fully resolved coincidence measurement has not yet been performed. Presently, coincidence studies at surfaces have been realized using spin polarized and unpolarized electron beams (see, for example, Ref. [8] and references therein). On the other hand, it has been demonstrated [9] that kinematically fully determined ion-atom coincident studies are feasible and yield a wealth of information on how electrons are excited and emitted. Thus, it seems timely to consider theoretically the ion-induced electron emission from surfaces involving kinematically determined coincidence measurements and to explore some of the information that can be extracted from these experiments.

Using ions for the study of electronic excitations of solid targets is a complementary tool to existing spectroscopic techniques, such as single photoemission spectroscopy [10] and electron-beam based spectroscopies [8]. In contrast to photons, the incoming ion may involve large momentum transfer to the surface, and in contrast to projectile electrons, the exchange process between the ion and the surface electrons is absent. At the same time, for ions an additional channel opens, namely, electron (radiative and nonradiative) capture [11] or even ion neutralization [12]. This channel may alternatively be excluded or studied in detail by resolving the charge state of the scattered ion. If the ion is fast, compared to the Fermi velocity, the kinetic emission channel [7,13] prevails over the charge transfer (capture or neutralization) one. This observation and the use of charge-state resolved coincidence measurements provide the basis for the investigation of the electronic properties of the target. For interpretation of the outcome of such coincidence experiments a theoretical model is needed that unravels the interplay between the effects related to the target electronic structure (structural factor) and those connected with the dynamical ion-electron collision (dynamical factor).

An adequate theory for the description of ion-induced electron emission from surfaces has to account for (a) the screening of the ion-electron interaction due to the surrounding medium, (b) the reflection of the ion beam from the surface, and (c) the diffraction and refraction of the electron wave at the surface as well as its damping inside the surface. It is the aim of this paper to develop and apply a quantum mechanical model which includes all these facets in a consistent way without resorting to phenomenological tools.

In short, the model is constructed as follows: (i) all the above mentioned processes are incorporated in one quantum mechanical amplitude, (ii) the screening by the medium is taken into account through renormalization of the bare ion-electron interaction using a surface dielectric function, and (iii) the scattering of charged particles (ions and electrons) from the surface is described using nonoverlapping muffin-tin surface ionic-core potentials. The latter are derived from *ab initio* calculations based on density functional theory within the local density approximation. Specific approximations concerning the numerical realization are presented below along with numerical results for the archetypical case, namely, proton impact on a clean flat aluminum surface. Numerical results for the electron energy and angle distributions are presented and analyzed for different proton scattering geometries. In addition, cross sections integrated over the final-state energy of the proton have been obtained. The role of screening effects and of the target electronic structure are investigated and conclusions about the perspectives of ion-beam based spectroscopy are made.

The paper is organized as follows. In Sec. II a general theoretical formalism is given and the approximations to the

*Electronic address: kouzakov@mpi-halle.de

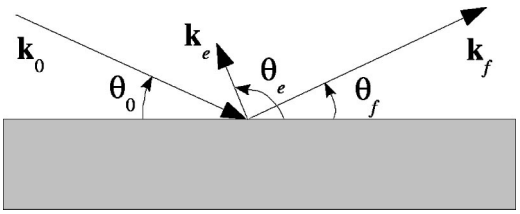

FIG. 1. Schematic drawing of the scattering geometry. The scattering plane is perpendicular to the surface. The angles of the particles are defined with respect to the surface as indicated by the arrows.

collision dynamics depending on the kinematical regime are specified. The numerical results for the case of proton impact on an aluminum surface are presented in Sec. III and the conclusions are drawn in Sec. IV. Atomic units (a.u.) are used throughout.

II. THEORETICAL MODEL

A. General formulation

The process under consideration is as follows. An ion A that has a momentum $\mathbf{k}_0$ and an energy $E_0=k_0^2/2M$ (M is the ionic mass) impinges from the vacuum onto a clean, ordered surface of a semi-infinite solid target. Among the various excitation processes induced by ion scattering we consider the electron emission process. Specifically, we study the reaction where the ion scattering state with momentum $\mathbf{k}_f$ and energy $E_f=k_f^2/2M$ is measured in coincidence with the emitted electron state. The latter is characterized by an electron momentum $\mathbf{k}_e$ and by the corresponding electron energy E_e (see Fig. 1). In spherical coordinates the momentum vectors $\mathbf{k}_f$ and $\mathbf{k}_e$ are specified by the solid angles Ω_f and Ω_e. In the frozen-core approximation, the fully resolved coincidence cross section has the form [14]

$$\frac{d\sigma}{dE_f dE_e d\Omega_f d\Omega_e}=\frac{M^2 k_f k_e}{(2\pi)^5 k_0}\sum_{i_{occ}}|\langle \mathbf{k}_f,\mathbf{k}_e|T|\mathbf{k}_0,i\rangle|^2 \times\delta(E_f+E_e-E_0-\varepsilon_i), \tag{1}$$

where the sum is taken over all occupied bound one-electron states with energy $\varepsilon_i=E_f+E_e-E_0$. T stands for an effective scattering t operator. It is defined as follows:

$$T=V_A+W_{eA}+(V_A+V_e+W_{eA})G_{eA}^+(E_{tot})(V_A+W_{eA}), \tag{2}$$

where V_A, V_e, and W_{eA} are the effective (optical) ion-solid, electron-solid, and ion-electron potentials, respectively, and $G_{eA}^+(E_{tot})$ is the ion-electron Green's operator involving the potential $V_A+V_e+W_{eA}$ at the total energy $E_{tot}=E_f+E_e$.

B. Ion-electron collision

In this work, we consider cases where the ion is fast compared to the Fermi velocity. The evaluation of Eq. (2) can then be performed by making similar approximations as in the case of high-energy electron-impact electron emission from surfaces [15,16]. Specifically, the electron-ion scattering (mediated by the potential W_{eA}) is treated in the Born approximation, which is justified by both the high velocity of the ion and the screening of the ion-electron potential by the surrounding medium. Thus Eq. (2) takes the form

$$T=[\mathbb{1}+V_e G_e^+(E_e)][\mathbb{1}+V_A G_A^+(E_f)]W_{eA}[\mathbb{1}+G_A^+(E_0)V_A], \tag{3}$$

where $G_e^+(E_e)$ is the electron-surface Green's operator evaluated at the energy E_e and accounting for multiple scattering from the potential V_e. The ion-surface Green's operator $G_A^+(E)$ describes the scattering processes from the potential V_A at the energy E.

The effective ion-electron scattering potential W_{eA} is deduced from the bare (undressed) potential $W_{eA}^{(0)}$ as

$$W_{eA}(\mathbf{r}_e,\mathbf{r}_A)=\frac{W_{eA}^{(0)}(\mathbf{r}_e-\mathbf{r}_A)}{\epsilon(\mathbf{r}_{e,\parallel}-\mathbf{r}_{A,\parallel},r_{e,\perp},r_{A,\perp},\omega)}, \tag{4}$$

where $\mathbf{r}_\parallel$ ($\mathbf{r}_\perp$) stands for the coordinate parallel (perpendicular) to the surface, ϵ is the dielectric function, and $\omega=E_0-E_f$.

C. Ion- and electron-solid scattering

As mentioned above we consider clean, ordered solid targets, in which case the crystal potential V_e (V_A) can be approximated by a superposition of nonoverlapping muffin-tin ionic potentials [14]:

$$V_{e/A}(\mathbf{r}_{e/A,\parallel},r_{e/A,\perp})=\sum_l\sum_j V_{e/A}^{(l,j)}\equiv\sum_l\sum_j V_{e/A}^{ion}(\mathbf{r}_{e/A,\parallel}-\mathbf{R}_{\parallel,j}^l,r_{e/A,\perp}-R_{\perp,l}). \tag{5}$$

The coordinate $R_{\perp,l}$ specifies the transverse position of the lth atomic layer parallel to the surface, whereas the two-dimensional vector $\mathbf{R}_{\parallel,j}^l$ characterizes the lateral position of lattice site j in the atomic layer l. The one-particle scattering states under the action of the potential (5),

$$|\psi_{\mathbf{k}_e}^-\rangle=[\mathbb{1}+G_e^-(E_e)V_e]|\mathbf{k}_e\rangle,$$

$$|\psi_{\mathbf{k}_f}^-\rangle=[\mathbb{1}+G_A^-(E_f)V_A]|\mathbf{k}_f\rangle,$$

$$|\psi_{\mathbf{k}_0}^+\rangle=[\mathbb{1}+G_A^+(E_0)V_A]|\mathbf{k}_0\rangle,$$

can be calculated using dynamical diffraction theory [17]. In particular, the high-energy approximation [18] can be employed for evaluation of the ionic scattering states. Due to the translational symmetry parallel to the surface of the potential (5), the surface-parallel components of the wave vectors of scattered particles (electrons or ions) are conserved, up to a multiple of the surface reciprocal lattice vector $\mathbf{g}_\parallel$. Therefore from Eqs. (4) and (5) one deduces the following important conservation rule for the sum surface-parallel momentum of the ion and the electron:

$$\mathbf{k}_{0,\parallel}+\mathbf{k}_{i,\parallel}=\mathbf{k}_{f,\parallel}+\mathbf{k}_{e,\parallel}+\mathbf{g}_\parallel, \tag{6}$$

where $\mathbf{k}_{i,\parallel}$ is the surface-parallel wave vector of the bound electron before the collision with the ion.

D. Specific approximations

For the numerical calculations presented in the next section we choose situations of nongrazing incidence and where the ion in the final state is detected at relatively large scattering angles (with respect to the surface). This allows us to use specific approximations in the numerical treatment of ion-electron and ion-solid collisions.

1. Ion-electron interaction

In the nongrazing incidence mode the incoming ion penetrates the surface deeply and therefore the surface dielectric function may be approximated in the numerical calculations by the bulk one (that of the infinite solid), i.e.,

$$W_{eA}(\mathbf{r}_e,\mathbf{r}_A)\approx\frac{W_{eA}^{(0)}(\mathbf{r}_e-\mathbf{r}_A)}{\epsilon(\mathbf{r}_e-\mathbf{r}_A,\omega)}. \tag{7}$$

2. Ion-solid scattering

In this case, the subsequent scattering of the fast ion off the muffin-tin ionic potentials centered at different sites [see Eq. (5)], and in particular the subsequent glancing angle collisions with the surface ionic cores that under grazing incidence may lead to surface channeling [19], are of less importance for the evaluation of the transition terms in Eq. (3) due to the potential W_{eA}. Therefore, in the present numerical calculations, only the terms corresponding to single-site multiple scattering off the muffin-tin ionic potentials before or after the collision with the electron are included. Thus Eq. (3) reduces to

$$T=[\mathbb{1}+V_eG_e^+(E_e)][T_A(E_f)g_A^+(E_f)W_{eA} + W_{eA}g_A^+(E_0)T_A(E_0)], \tag{8}$$

where $g_A^+(E)$ is the free ion–surface Green's operator at the energy E and, in accordance with Eq. (5), the t operator T_A is given by the relations

$$T_A=\sum_l\sum_j T_A^{(l,j)},\quad T_A^{(l,j)}=V_A^{(l,j)}+V_A^{(l,j)}g_A^+T_A^{(l,j)}. \tag{9}$$

This amounts to the single-site impulse approximation [20].

The direct transition term

$$[\mathbb{1}+V_eG_e^+(E_e)]W_{eA}$$

is excluded from Eq. (8) because its contribution is negligible and, in particular, it cannot account for the ion reflection at the surface. However, this term may have a significant contribution in the transmission mode setup, which case we do not consider in detail here.

3. Fully resolved cross section

Using Eq. (8), we can rewrite Eq. (1) as follows:

$$\frac{d\sigma}{dE_fdE_ed\Omega_fd\Omega_e}=\frac{M^2k_fk_e}{(2\pi)^5k_0}\sum_{i_{occ}}|\langle\psi_{\mathbf{k}_e}^-|T_{\mathbf{k}_f\mathbf{k}_0}|\psi_i\rangle|^2\delta(\varepsilon-\varepsilon_i), \tag{10}$$

where $\varepsilon=E_f+E_e-E_0$ and

$$T_{\mathbf{k}_f\mathbf{k}_0}=\langle\mathbf{k}_f|T_A(E_f)g_A^+(E_f)W_{eA}+W_{eA}g_A^+(E_0)T_A(E_0)|\mathbf{k}_0\rangle \tag{11}$$

is an effective one-electron transition operator. It can be seen that, except for the transition operator, the formula (10) is similar to the expression given by the golden rule for the angle- and energy-resolved photocurrent as well as to that for high-energy electron-impact electron emission [15]. Thus, one can implement the well-developed algorithms of the one-step model of photoemission [21] for evaluation of Eq. (10).

III. NUMERICAL REALIZATION

In this section we present numerical results for the energy and angular distributions of the electrons emitted from a clean aluminum surface upon the impact of protons. Two possible geometries of the proton scattering at the surface are considered (see Fig. 1), namely, the specular ($\theta_0=\theta_f$) and the nonspecular ($\theta_0\neq\theta_f$) reflection modes. The ingredients of the numerical scheme are as follows.

(1) The ionic muffin-tin potentials $V_A^{(l,j)}$ are derived from *ab initio* Korringa-Kohn-Rostoker band-structure calculations based on the local density approximation within the density functional theory [22]. The on-site t matrices are evaluated in the first Born approximation with respect to the involved potential, i.e., we set $T_A^{(l,j)}=V_A^{(l,j)}$ (this amounts to the so-called kinematical approximation).

(2) For s-p bonded metals like aluminum, the electronic states $|\psi_i\rangle$ and $|\psi_{\mathbf{k}_e}^-\rangle$ are (for our purpose) satisfactorily approximated by those of a jellium model, i.e., by the eigenstates of a steplike potential V_e that vanishes in the vacuum and inside the semi-infinite solid takes on the value $V_e=-\varepsilon_F-\Phi$, where ε_F and Φ are the Fermi energy and the work function, respectively. The electron motion parallel to the surface is thus free (see Ref. [15] for details).

(3) The proton-electron interaction is employed in the approximate form (7). To investigate the effects of the static and dynamical screening on the electron emission, the (static) Thomas-Fermi (TF) [23] and the modified (dynamical) Lindhard-Mermin (LM) dielectric functions [24,25] are used.

The TF dielectric function is energy independent; in momentum space it is given by the simple formula [23]

$$\epsilon(q,\omega)=1+\frac{\lambda^2}{q^2}, \tag{12}$$

where λ is the screening length. In contrast to the static TF model of screening, the LM function takes account of the dynamical screening and has a more complex structure [25], explicitly given as follows:

$$\epsilon(q,\omega+i\Gamma)=1+N/D,$$

$$N=(\omega+i\Gamma)[\epsilon_L(q,\omega+i\Gamma)-1+4\pi\chi_{core}],$$

$$D=\omega\{1-G(q)[\epsilon_L(q,\omega+i\Gamma)-1]\}+i\Gamma\{1-G(q)[\epsilon_L(q,0)-1]\}\frac{\epsilon_L(q,\omega+i\Gamma)-1+4\pi\chi_{core}}{\epsilon_L(q,0)-1+4\pi\chi_{core}}. \quad (13)$$

The Lindhard dielectric function [26] occurring in the above relations has the form

$$\epsilon_L(q,\omega)=1+\frac{3}{128\alpha^2Z^3}\left\{4Z+[1-(U-Z)^2]\ln\frac{U-Z-1}{U-Z+1}-[1-(U+Z)^2]\ln\frac{U+Z-1}{U+Z+1}\right\}, \quad (14)$$

where

$$Z=q/2k_F, \quad U=\omega/4Z\varepsilon_F.$$

The Fermi momentum is denoted by k_F. The function α that appears in Eq. (14) is given by $\alpha=\varepsilon_F/\omega_{pl}$, where ω_{pl} is the plasma frequency. For aluminum, the parameters in Eq. (13) are given by [24]

$$\Gamma=(0.53+30.9Z^2 \text{ eV})\Theta(0.067-Z^2)+(2.6+0.2 \text{ eV})\Theta(Z^2-0.067),$$

$$G=2.5Z^2-i[2.12Z^2\Theta(0.067-Z^2)+0.142\Theta(Z^2-0.067)],$$

$$4\pi\chi_{core}=0.05, \quad (15)$$

where Θ is the step function.

A. Fully resolved cross sections for proton scattering from aluminum

1. Electron energy distributions

Figure 2(a) shows the energy distribution of the electrons emitted normal to the surface following the specular reflection of protons from an aluminum (001) single-crystal surface. The cross section diminishes with vanishing electron energy E_e. This is due to the kinematical factor (k_e) that appears in Eq. (1). The shape of the energy distribution curve is directly related to the Fourier transform of the electron-ion interaction potential (the form factor). Since this potential is renormalized differently when using either the TF or the LM model of screening, we observe marked differences. First, the calculated electron intensity using the LM dielectric function [Eq. (13)] is two orders of magnitude larger than in the case of the TF dielectric function [Eq. (12)]. Second, in the LM results the electron energy distribution exhibits a peak at an emission energy $E_e\approx\omega_{pl}-\Phi$. The position and the width of the peak are directly related to, respectively, the plasmon pole and the plasmon lifetime. These features are beyond the scope of the TF theory of screening and hence they do not show up in the TF cross section results.

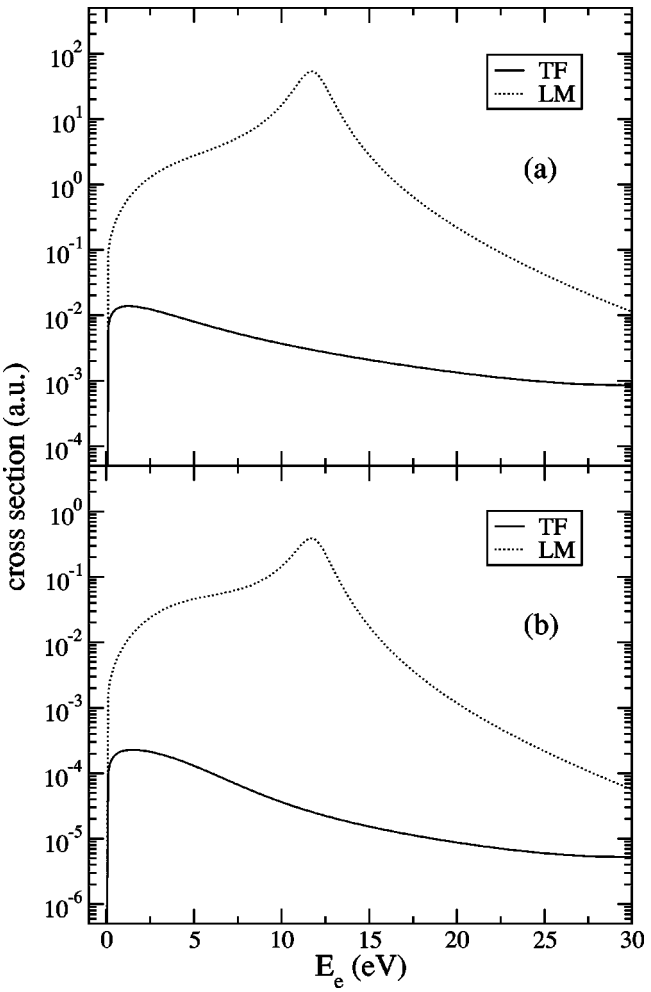

FIG. 2. The energy distribution of the electrons emitted normal to the (001) fcc face of aluminum in the case of the (a) specular ($\theta_0=\theta_f=15°$) and (b) nonspecular ($\theta_0=75°$, $\theta_f=15°$) reflection mode. The initial and final proton energies are $E_0=100$ keV and $E_f=E_0-E_e-\Phi$, respectively.

We recall that the plasmon wave vector is rather small (<1 a.u.). Thus, the appearance of the ''plasmon feature'' in the electron energy distribution when employing the LM dielectric function (14) indicates that the momentum transferred by the proton to the electron is small. Nevertheless, the momentum transferred by the projectile to the target as a whole is large. This momentum is mainly absorbed by the surface-parallel atomic planes before and/or after the proton-electron collision. In the case of the nonspecular reflection mode, the momentum transfer to the surface-parallel atomic layers is accompanied by a momentum transfer to the surface-perpendicular planes. The momentum transferred to the ejected electron can also be small in this case. Therefore, for the (proton) nonspecular reflection mode we may expect plasmon-associated features in the electron spectra. In fact, as shown in Figs. 2(a) and 2(b), the energy distributions of

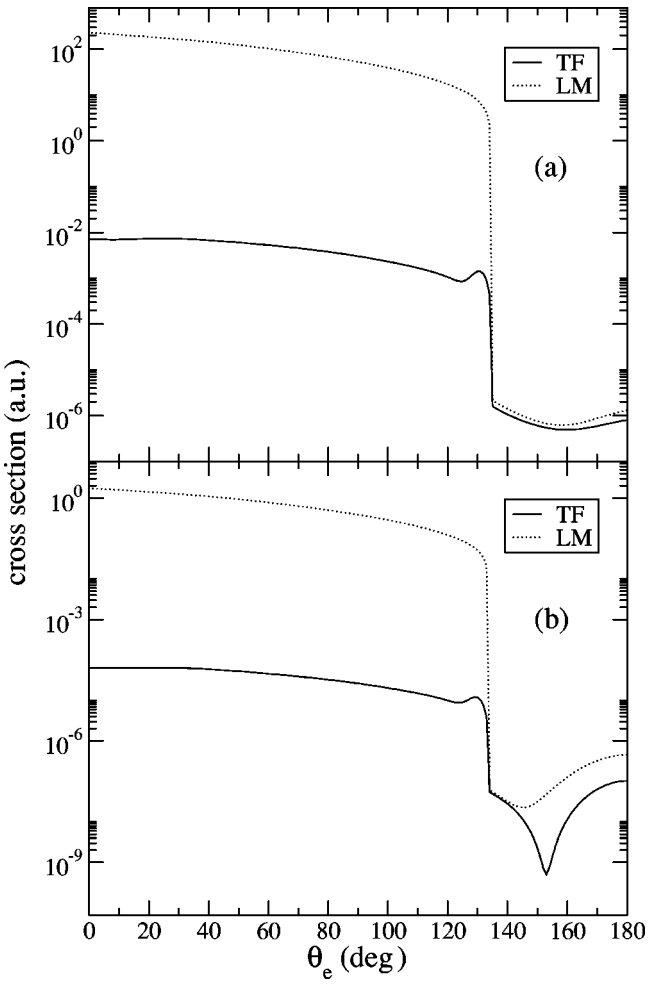

FIG. 3. The angular distribution of electrons (with respect to the [100] direction) emitted with energy $E_e=\omega_{pl}-\Phi$ in the case of (a) specular and (b) nonspecular reflection modes.

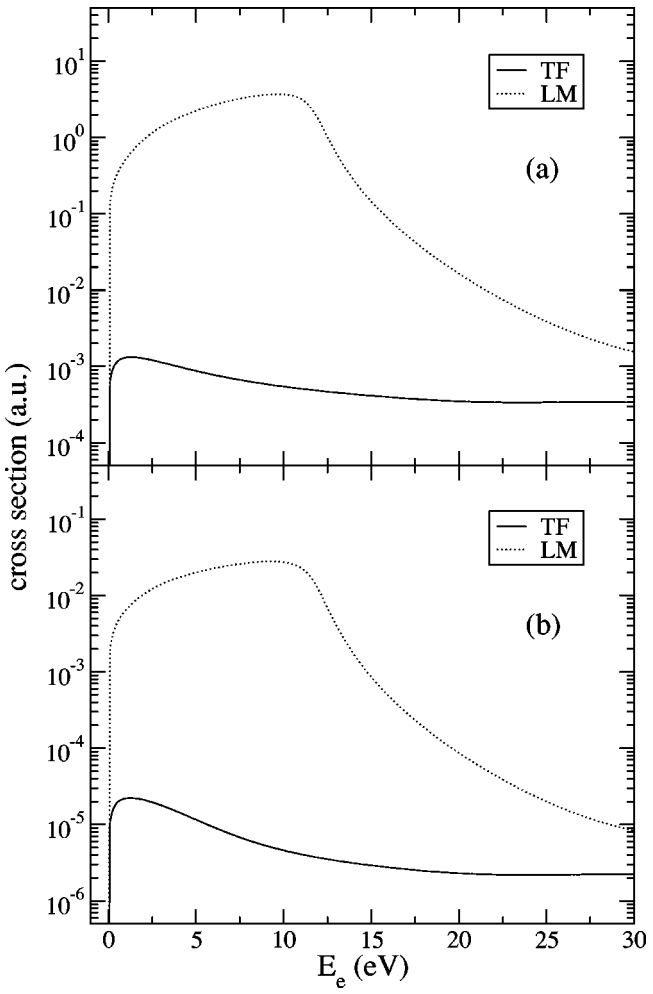

FIG. 4. The same as in (a) Fig. 2(a) and (b) Fig. 2(b), but integrated over the final proton energy E_f.

the electrons emitted normally to the surface have almost the same shape for both the specular and the nonspecular reflection modes of the projectile. In the latter case, however, the cross sections are two orders of magnitude smaller than in the case of the projectile specular scattering, which can be traced back to the smaller probability of proton scattering through larger angles.

2. Electron angular distributions

Figure 3 shows the angular distribution of electrons in the case of $E_f=E_0-\omega_{pl}$, i.e., for the electron energies where the (LM) theoretical electron emission intensity is largest. An abrupt drop in the cross section is observed at about $\theta_e=130°$ for both modes of the proton scattering geometry. This feature emerges as a consequence of the condition

$$k_F \geqslant |\mathbf{k}_{f,\|}-\mathbf{k}_{0,\|}+\mathbf{k}_{e,\|}+\mathbf{g}_\||, \tag{16}$$

which can be derived from Eq. (6). The condition (16) marks the crossing of the Fermi surface when scanning the wave vector $k_{e,\|}$. In this context it should be noted that in the case of the specular reflection mode $|\mathbf{k}_{f,\|}-\mathbf{k}_{0,\|}|\sim 0.1$ a.u., while in the case of the nonspecular reflection mode $|\mathbf{k}_{f,\|}-\mathbf{k}_{0,\|}|$ $\sim 10^3$ a.u. Considering that $k_{e,\|}<1$ a.u., we remark that combined proton-electron diffraction with a large reciprocal lattice vector $g_\|$ is important to compensate for surface-parallel momentum transfer in the nonspecular reflection mode. Since we assume here a perfect energy and angular resolution and as we do not include in our calculations the effects of a finite lifetime for the bound electron states, the observed cross section drop due to the crossing of the Fermi surface is very sharp.

B. Integral cross sections

The results for the electron spectra shown in Figs. 2 and 3 have been calculated assuming a perfect resolution of the proton energy. Experimentally, exact determination of the proton energy is difficult to realize. Therefore, it is of interest to inspect the electron spectra where the projectile final-state energy is not resolved [27]. This means we integrate Eq. (10) over the energy of the scattered projectile E_f. The energy and angular distributions integrated over the final proton energy are shown in Figs. 4 and 5. The scattering geometry in Figs. 4 and 5 is identical to that chosen in Figs. 2 and 3,

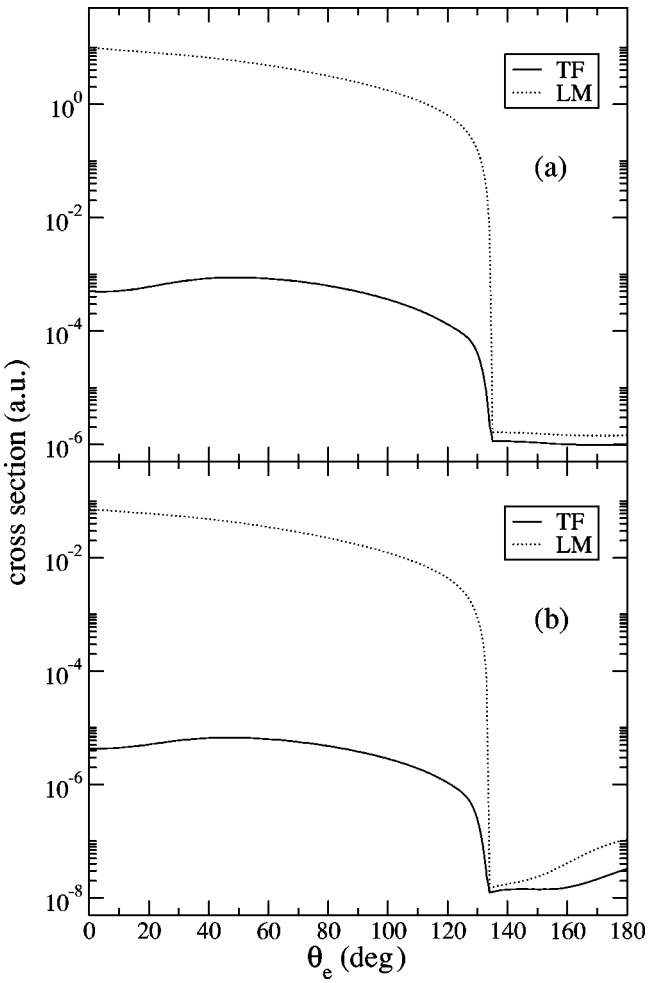

FIG. 5. The same as in (a) Fig. 3(a) and (b) Fig. 3(b), but integrated over the final proton energy E_f.

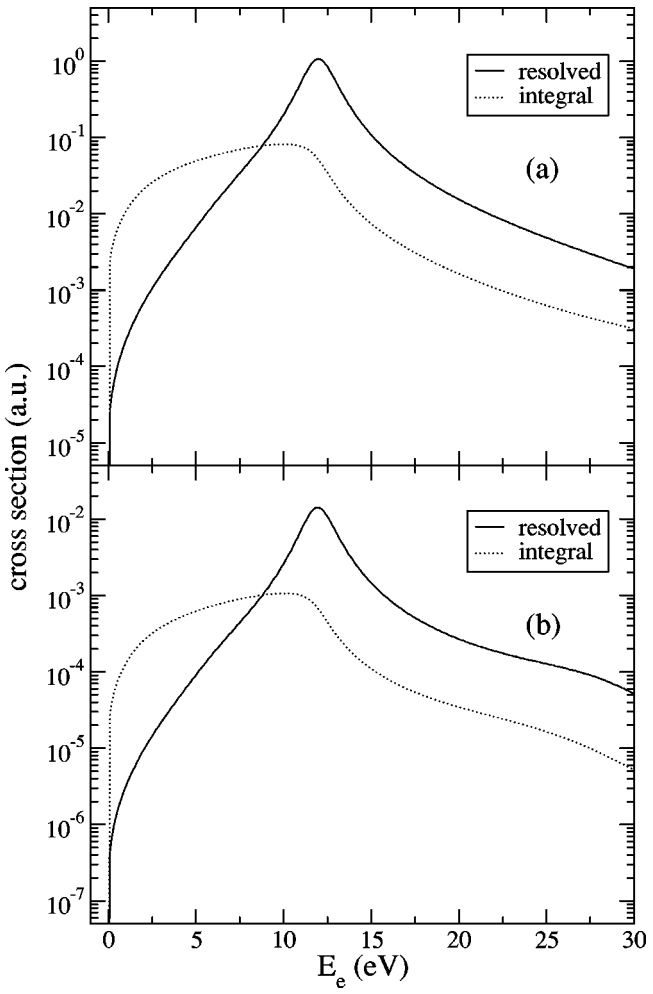

FIG. 6. The electron energy distributions at incident proton energy $E_0=400$ keV in the case of the LM dielectric function. The conditions for the resolved and integral cases are the same as in (a) Figs. 2(a) and 4(a), respectively, and (b) Figs. 2(b) and 4(b), respectively.

respectively. As is clear from a comparison of Figs. 2 and 4, the ''plasmon feature'' is smeared out if the final-state energy of the proton is not resolved. Moreover, the inelastic energy losses of the electrons on their way to the detector, which are not included in the present calculations, can in fact completely smear out the ''plasmon feature'' and make the shape of the energy distribution curve for the LM function similar to that for the TF function. On the other hand, the angular distributions are close to those in Fig. 3. In particular, the feature pertinent to the Fermi surface crossing is preserved. However, the cut of the angular distributions is smoother now.

C. Effect of proton velocity on electron energy distributions

Figure 6 shows the results for the electron energy distributions using the LM dielectric function only [28]. The incident proton energy is $E_0=400$ keV. It can be seen that the electron emission cross sections are considerably smaller than in the case where $E_0=100$ keV. This is because of the increased transferred momentum. The cross section for the case of well-resolved proton energy in the final state shows a much stronger pronounced ''plasmon feature.'' This can be explained using a simplified kinematical model of the proton-electron collision: If a proton in a collision with an electron (assumed at rest) transfers the momentum **q**, then the transferred energy is given by $\Delta E=\mathbf{v}\cdot\mathbf{q}$, where **v** is the proton velocity. Thus, the larger the proton velocity, the smaller the momentum transfer required at a given energy transfer. Since the effect of the plasmon decay in the LM dielectric function decreases with decreasing q, the peak in the electron energy distribution at $E_e\approx\omega_{pl}-\Phi$ ($\Delta E\approx\omega_{pl}$) becomes sharper at larger proton velocities.

IV. SUMMARY AND CONCLUSIONS

In the case when the final-state energy of the proton is resolved, all the results for the energy distributions using the LM dielectric function exhibit a peak at the electron energy $E_e=\omega_{pl}-\Phi$. The width of this peak is related to the decay of the plasmon as follows: the larger the lifetime of the plasmon, the stronger and the narrower the peak becomes. The electron emission can thus be viewed as the decay of the plasmon excited by the proton impact. However, such a scenario for this process is true only if the electron is ejected

from the Fermi level. In the case of unresolved final-state proton energy, the ''plasmon feature'' is smeared out, because at given electron energy E_e all the bound states contribute effectively to the ejection process, including the state at the Fermi level.

It is useful to compare the results for the angular distributions with qualitative predictions of the simple classical model based on kinematical considerations. According to this model, the proton moves along straight lines before and after the collision with the surface ionic cores. The ejection of an electron takes place during this motion and if the electron energy is low it does not affect the classical proton trajectory. Restricting consideration to a single collision of the proton with the surface ionic cores, one would expect the electrons to be ejected preferably in the directions perpendicular to the directions of the incident and final proton velocities. As can be seen in Figs. 3 and 5, this conclusion does not hold true. Rather, it is deduced that there is no preferential direction for the electron ejection, when the surface momentum components of the initially bound electron are less than the Fermi momentum. We recall that the present calculations do not account for cascade multiplication processes, which generally lead to uniform angular distributions of the emitted electrons [19]. Thus, we can conclude that in our particular case the dynamics rather than the kinematics is important. This dynamics is included through the matrix elements given by Eq. (10).

In summary, we have constructed a theoretical model for single-electron emission upon the impact of fast ions on ordered crystalline surfaces. The model accounts for the electronic dielectric response of the surface as well as for the propagation of the ionic beam inside the surface and for the diffraction of the ejected electron wave. All these processes are incorporated in a single quantum mechanical amplitude. Approximations for specific situations have been derived. The model can be extended to the case of substitutionally disordered surfaces in a similar way to that proposed for the case of high-energy electron-impact electron emission from surfaces of random alloys [15].

Numerical calculations have been performed for the case of proton impact on an aluminum surface for different scattering geometries. A plasmon feature has been identified in the electron energy distributions when the proton energy in the final state is well resolved. If the proton energy is not well resolved the plasmon peak is smeared out substantially. The signature of Fermi surface crossing has been identified in the electron angular distributions. The present particular theoretical findings indicate the potential for utilizing ion-induced single-electron emission for studies of the electronic properties of surfaces.

[1] M. Kaminski, *Atomic and Ionic Impact Phenomena on Metal Surfaces* (Springer, Berlin, 1965).

[2] M. Rösler, in *Particle Induced Electron Emission I*, Vol. 122 of Springer Tracts in Modern Physics (Springer, Berlin, 1991).

[3] *Ionization of Solids by Heavy Particles*, edited by R.A. Baragiola (Plenum, New York, 1993).

[4] S. Bartholomé, A. Dubus, J. Devooght, J.-P. Ganachaud, and C. Attard, Nucl. Instrum. Methods Phys. Res. B **125**, 13 (1997).

[5] L. Ding, J.M. Woolsey, G. Libiseller, C. McGrath, M.B. Shah, R.W. McCullough, and J. Geddes, Philos. Trans. R. Soc. London, Ser. A **357**, 1381 (1999).

[6] K. Kimura, G. Andou, and K. Nakajima, Nucl. Instrum. Methods Phys. Res. B **164-165**, 933 (2000).

[7] H. Winter, H. Eder, F. Aumayr, J. Lörincik, and Z. Sroubek, Nucl. Instrum. Methods Phys. Res. B **182**, 15 (2001).

[8] *Many Particle Spectroscopy of Atoms, Molecules, Clusters, and Surfaces*, edited by J. Berakdar and J. Kirschner (Plenum, New York, 2001).

[9] J. Ullrich, R. Moshammer, R. Dörner, O. Jagutzki, V. Mergel, H. Schmidt-Böcking, and L. Spielberger, J. Phys. B **30**, 2917 (1997).

[10] S. Hüfner, *Photoelectron Spectroscopy: Principles and Applications* (Springer, Berlin, 1995).

[11] M. Maazouz, L. Guillemot, and V.A. Esaulov, Phys. Rev. B **56**, 9267 (1997); M. Maazouz, L. Guillemot, V.A. Esaulov, and D.J. O'Connor, Surf. Sci. **398**, 49 (1998); R. Souda and M. Kato, *ibid.* **496**, 231 (2002).

[12] R. Zimny, Surf. Sci. **233**, 333 (1990); R. Souda, K. Yamamoto, B. Tilley, W. Hayami, T. Aizawa, and Y. Ishizawa, Phys. Rev. B **50**, 18 489 (1994); M. Kato, D.J. O'Connor, K. Yamamoto, and R. Souda, Surf. Sci. **363**, 150 (1996).

[13] B. van Someren, A. Zeijlmans van Emmichoven, I.F. Urazgil'din, and A. Niehaus, Phys. Rev. A **61**, 032902 (2000).

[14] J. Berakdar and M.P. Das, Phys. Rev. A **56**, 1403 (1997).

[15] K.A. Kouzakov and J. Berakdar, Phys. Rev. B **66**, 235114 (2002).

[16] K.A. Kouzakov and J. Berakdar, J. Phys.: Condens. Matter **15**, L41 (2003).

[17] M.A. van Hove, W.H. Weinberg, and C.-M. Chan, *Low Energy Electron Diffraction. Experiment, Theory and Surface Structure Determination* (Springer, Berlin 1986).

[18] H.S. Kim and S.S. Sheinin, Phys. Status Solidi B **109**, 807 (1982); L.J. Allen, I.E. McCarthy, V.W. Maslen, and C.J. Rossouw, Aust. J. Phys. **43**, 453 (1990).

[19] H. Winter, Phys. Rep. **367**, 387 (2002).

[20] P. Weinberger, *Electron Scattering Theory for Ordered and Disordered Matter* (Clarendon Press, Oxford, 1990).

[21] J.B. Pendry, Surf. Sci. **57**, 679 (1976).

[22] A. Gonis, *Theoretical Materials Science: Tracing the Electronic Origins of Materials Behavior* (Materials Research Society, Warrendale, PA, 2000).

[23] N.W. Ashcroft and N.D. Mermin, *Solid State Physics* (Hault-Saunders, Tokyo, 1981).

[24] P.C. Gibbons, S.E. Schnatterly, J.J. Ritsko, and R. Fields, Phys. Rev. B **6**, 2451 (1976).

[25] V.U. Nazarov, Phys. Rev. B **56**, 2198 (1997).

[26] J. Lindhard, K. Dan. Vidensk. Selsk. Mat. Fys. Medd. **28**, No.8 (1954); A.J. Glick and R.A. Ferrell, Ann. Phys. (N.Y.) **11**, 359 (1960).

[27] More specifically, we assume that the energy resolution is larger than the energy width of the conduction band ($\sim$10 eV), but still high enough to rule out electron emission from the core levels $2s$ and $2p$, which have ionization potentials 77 eV and 124 eV, respectively.

[28] In the usual units for cross sections, 1 a.u. corresponds to approximately 3.8×10^{-20} cm^2 eV^{-2} sr^{-2} in the resolved case and to approximately 10^{-18} cm^2 eV^{-1} sr^{-2} in the integral case.